Succinate is Broadly Tissue-Permeant and Uncouples Mitochondrial Respiration from ATP Synthesis

Daniel T. Hass[1], Brian M. Robbings[1,2], Celia M. Bisbach[1], Elizabeth Giering[3], Thomas O. Mundinger[3], Martin Sadilek[4], Ian R. Sweet[2], James B. Hurley[1*]

[1]*Biochemistry Department, The University of Washington, Seattle WA 98109*
[2]*Diabetes Institute, The University of Washington, Seattle WA 98109*
[3]*Division of Endocrinology/Metabolism, Veterans Affairs Puget Sound Health Care System, Seattle, WA*
[4]*Chemistry Department, The University of Washington, Seattle WA 98109*
*Corresponding Author

Email: jbhhh@uw.edu

Abstract

When tissues have limited access to O_2 the mitochondrial respiratory apparatus can reduce fumarate to succinate as a surrogate for reducing O_2 to H_2O. The succinate can be released from the tissue into the systemic circulation, but its metabolic fate in the body is mostly unknown. Using a combination of *ex vivo* and *in vivo* strategies we investigated the fate of circulating succinate in mice. We find that succinate from the blood is imported and oxidized by most tissues. Remarkably, succinate from the circulation can stimulate metabolic activity in most tissues, regardless of their energy demands, by uncoupling mitochondrial respiration from ATP synthesis. A notable exception is the retina, where carbons from succinate are incorporated into gluconeogenic intermediates.

Introduction

Oxidation of fuel by mitochondrial is vital for eukaryotic life. Transfer of electrons to O_2 to make H_2O is the driving force for oxidation of fuels. However, when O_2 is scarce, mitochondria instead transfer electrons to fumarate to make succinate (Chouchani et al., 2014; Hochachka et al., 1975).

Like H_2O, succinate is released into the circulation (Hochachka & Dressendorfer, 1976; Prag et al., 2020). Unlike H_2O, succinate retains metabolic energy that can be released by further oxidation. The metabolic fate of succinate released into the circulation is mostly unknown. Brown adipose tissue can use succinate to fuel thermogenesis (Mills et al., 2018) and succinate released from the mouse retina can be oxidized when it is taken up into the retinal pigment epithelium, an O_2-rich tissue (Bisbach et al., 2020).

Otherwise, the tissue specificity and downstream metabolism of circulating succinate are mostly unknown. Here we report the metabolic fate of systemic succinate in liver, lung, cerebellum, retina, eyecup, and adipose tissue. We find that most tissues can oxidize circulating succinate. A notable exception is the retina. ^{13}C tracing experiments indicate that succinate is anapleurotic to the retina and may contribute to the pool of gluconeogenic intermediates. Surprisingly, we also find that oxidation of succinate very effectively stimulates mitochondrial uncoupling.

Results

Extracellular Succinate Promotes O_2 Flux Ex Vivo

In the conventional Krebs cycle, succinate dehydrogenase oxidizes succinate to fumarate. The electrons from that reaction reduce coenzyme Q_{10}, cytochrome C, then O_2 (**Figure 1A**). Oxidation of succinate therefore stimulates O_2 consumption (OCR) by complex IV. We used a perifusion respirometer to quantify OCR that is inhibited by the complex IV inhibitor KCN. **Figure 1B** shows how OCR depends on succinate concentration. Increasing succinate concentrations (30 μM, 100 μM, 300 μM, 1 mM, 3 mM, 10 mM, 30 mM, and 100 mM all with 5 mM glucose present) stimulate OCR in liver, cerebellum, interscapular brown adipose tissue (BAT), kidney, eyecup (containing retinal pigment epithelium, choroid, and sclera), and retina tissue. The data are fit with an allosteric sigmoidal function (**Figure 1C-H, Table 1**). In most tissues, succinate enhances OCR with a best-fit V_{max} of 0.34-0.89 nmol O_2 / mg tissue / minute, and best-fit $K_{1/2}$ values ranged from 0.9-2.72 mM (**Table 1**), The retina lay far outside this range (V_{max} of 0.12 nmol O_2 / mg tissue / minute and $K_{1/2}$ of 8.9 mM). This dependence of OCR on succinate is an estimate because it did not reach saturation. This suggests either that in retinas there is unusually limited succinate

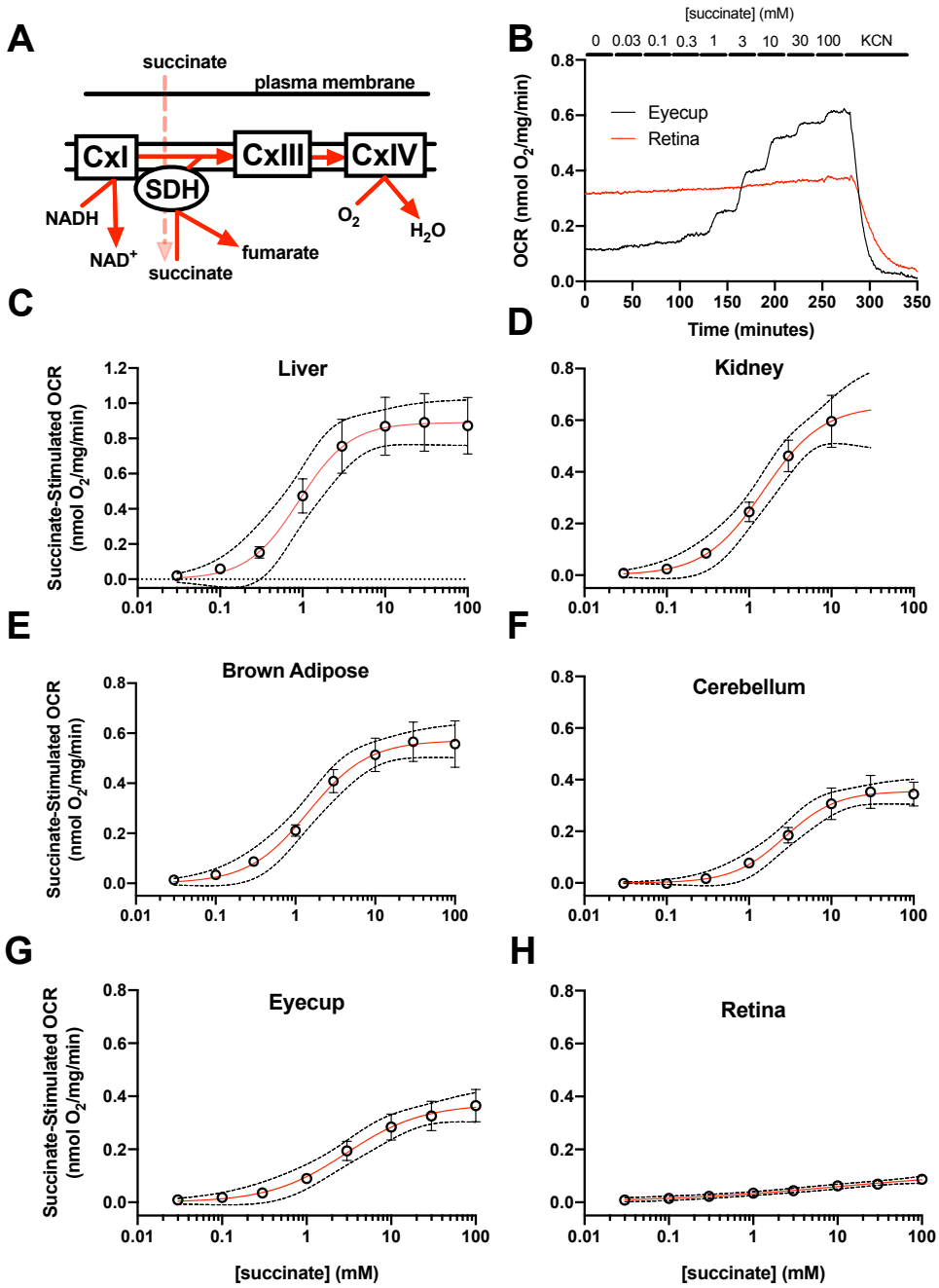

Figure 1. Extracellular Succinate Increases Oxygen Consumption in Diverse Tissues Ex Vivo. (**A**) Schematic of the mitochondrial electron transport chain. We measured O_2 consumption rate (OCR) in freshly dissected (**C**) liver (n=3), (**D**) kidney (n=4), (**E**) brown adipose (n=3)), (**F**) cerebellum (n=3), (**B,G**) eyecup (n=3), and (**B,H**) retina (n=4) tissue from C57BL6/J mice, respiring in KRB buffer with 5 mM glucose. We supplied this media with increasing concentrations of disodium succinate (30 μM, 100 μM, 300 μM, 1 mM, 3 mM, 10 mM, 30 mM, or 100 mM) and determined the OCR above the 5 mM glucose "baseline" respiration. Example experiments are shown in (**B**). Mean ± SEM steady state OCR as a function of [succinate] are summarized for different tissues in C-H -state. We fit the data with an allosteric sigmoidal curve (red lines). Best-fit parameters are available in **Table 1**. Dotted lines surrounding the curves represent 95% confidence intervals from the curve fit.

transport or that the ETC of the retina has an unusually poor ability to oxidize succinate. In all other tissues we studied, succinate clearly stimulates mitochondrial respiration.

Table 1. Best-Fit Kinetic Parameters for *ex vivo* Succinate oxidation

Least squares fit, Parameters are represented as [mean (95% Confidence Interval)]

Tissue	Basal OCR (nmol O_2 / mg / min)[&]	V_{max} (nmol O_2 / mg / min)	$K_{1/2}$ [succinate] (mM)	H*	R^2	n
Retina	0.31 (0.12-0.50)	0.12 (?**)	8.89 (1.06-?**)	0.42 (0.19-0.77)	0.81	4
Cerebellum	0.22 (0.07-0.37)	0.36 (0.31-0.42)	2.72 (1.67-4.94)	1.38 (0.81-2.73)	0.90	3
Eyecup	0.15 (0.06-0.24)	0.34 (0.28-0.46)	2.49 (1.33-8.31)	1.05 (0.55-2.24)	0.81	5
Liver	0.07 (-0.32-0.46)	0.89 (0.77-1.04)	0.90 (0.49-1.75)	1.40 (0.72-?**)	0.85	3
BAT	0.21 (0.12-0.30)	0.57 (0.51-0.66)	1.45 (0.9-2.58)	1.15 (0.72-2.04)	0.91	3
Kidney	0.48 (0.38-0.58)	0.66 (0.52-1.20)	1.50 (0.84-8.53)	1.21 (0.64-2.35)	0.88	4

* Hill's Slope

** "?" indicates that the curve fit is unable to estimate this parameter

The effect of succinate on OCR could be mediated by SUCNR1, a G-protein coupled receptor that stimulates activity of genes involved in systemic metabolism (Prag et al., 2020; Wang et al., 2020). We attempted to stimulate this receptor in eyecup tissue using the SUCNR1 agonist cis-epoxysuccinate (500 μM). This concentration of agonist should be as potent for SUCNR1 as 5 mM succinate (Geubelle et al., 2017), yet in the presence of glucose it did not stimulate O_2 consumption (**Figure S1**), indicating that effects of succinate on OCR are not due to signaling through SUCNR1.

Infused Succinate is Metabolized In Vivo

Ex vivo experiments provide important information, but the tissue isolation process may influence the integrity or metabolic activity of a tissue. To address the concern that our ex vivo OCR measurements were thus influenced, we evaluated import of succinate *in vivo* by infusing mice with a 100 mg/kg bolus of uniformly labeled (U)-^{13}C succinate dissolved in sterile saline (pH 7.4) through jugular vein catheters. Before infusion we withdrew two 10 μL baseline whole blood samples through a carotid catheter. After we infused labeled succinate through the jugular catheter we sampled 10 μL of blood at 0.5, 1, 2, 3, 4, 5, 7.5, and 10 minutes. These samples were analyzed using gas chromatography–mass spectrometry (GC-MS) to measure the accumulation of ^{13}C on metabolites in glycolysis and the Krebs cycle (**Table 2**). Total blood U-^{13}C-succinate levels (as m+4 because it contains four ^{13}C atoms) spiked immediately following infusion and rapidly declined throughout the 10-minute process (**Figure 2A**). A single exponential fit of m+4 succinate over time shows that infused succinate reached a half maximal concentration at 0.89 (95% CI: 0.6-1.31) minutes post-infusion. The dominant isotopologue in blood was m+4, showing that for at least 10 minutes following the bolus infusion, tissues have access to a pool of almost fully labeled succinate (**Figure 2B**). A molecule in blood spectrally overlaps with m+4 succinate and interferes with estimation of succinate isotopologue distribution in unlabeled blood samples. However, this 'm+4' contaminant was minor relative to the abundance of m+4 succinate following infusion. Following the infusion, m+4 labeling briefly appears in circulating fumarate and malate pools and is cleared by the time total m+4 succinate reaches a steady state in circulation (**Figure S2**).

We euthanized mice five minutes after the bolus infusion and quantified metabolites in the retina, cerebellum, eyecup, liver, lung, interscapular brown adipose tissue (BAT), and interscapular white adipose tissue (WAT). M+4 succinate was present in all tissues (**Figure 2C**), and in the retina

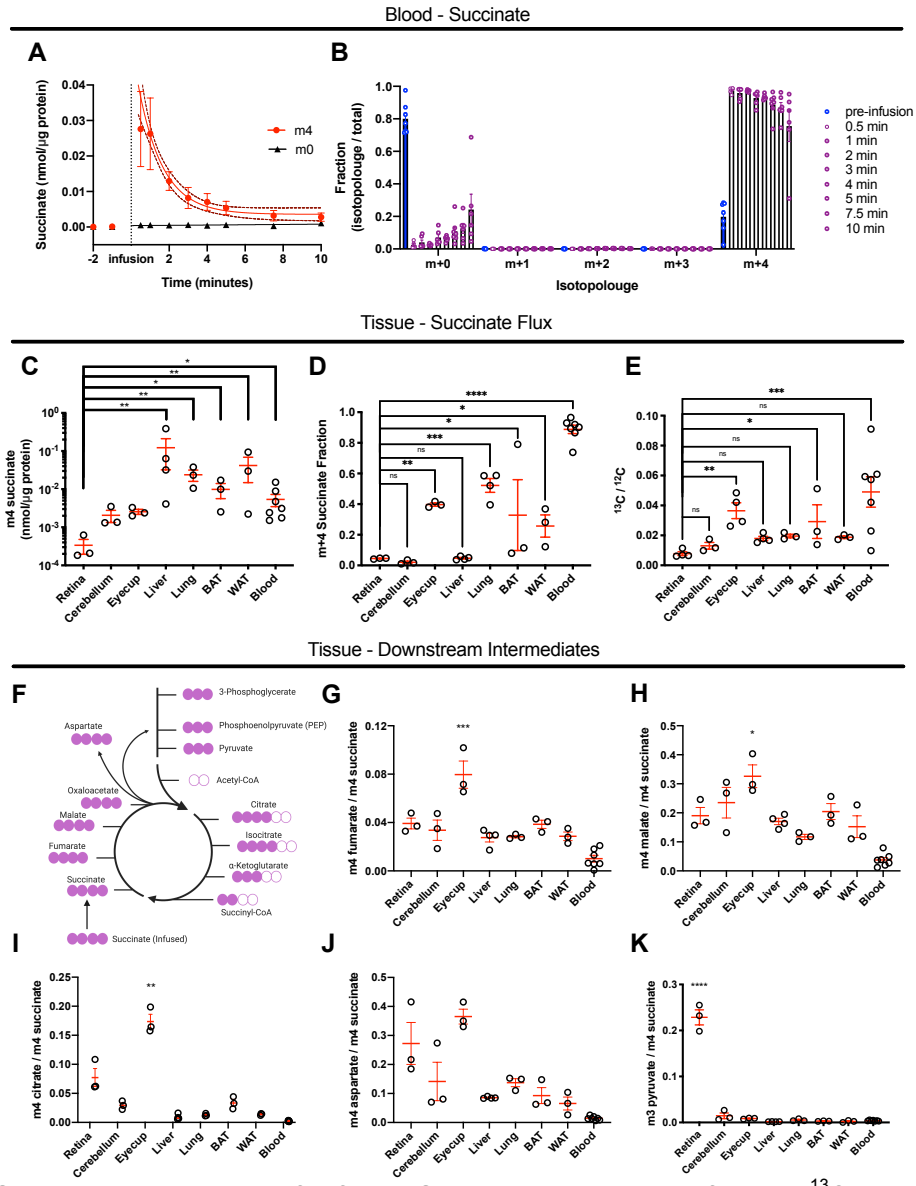

Figure 2. Systemic Metabolism of Infused Succinate. (**A-B**) We infused U-^{13}C-succinate into the mouse bloodstream and sampled blood 0.5 (n=5), 1 (n=5), 2 (n=7), 3 (n=6), 4 (n=5), 5 (n=7), 7.5 (n=6), and 10 (n=6) minutes post-infusion, with catheterized, uninfused mice as a "0 minute" control (n=7). **(A)** We measured unlabeled (m+0) and fully ^{13}C-labeled (m+4) succinate in blood post-infusion (plotted: mean ± SEM) and fit a one-phase decay function to the data (fit line ± 95% CI) **(B)** Isotopic abundance of blood succinate prior to (blue) and following (purple) infusion. Represented are individual replicates (dots) and mean ± SEM (bars). (**C-E**) Five minutes following the infusion, blood succinate is metabolized by retina (n=3), cerebellum (n=3), eyecup (n=3), liver (n=4), lung (n=3), BAT (n=3), WAT (n=3), and blood (n=7). (**C**) m+4 succinate concentration within tissues shows differential tissue entry. (**D**) Fractional labeling of m+4 succinate shows relative replacement of the succinate pool by labeled substrate five minutes following the infusion, and (**E**) ^{13}C/^{12}C is the relative extent to which measured Krebs cycle metabolites (any of which could be a product of ^{13}C-succinate; **Table 2**) are labeled by ^{13}C, relative to total ^{12}C abundance in that tissue. (**F**) represents succinate's position in the Krebs cycle and which carbons are labeled (purple filled circles) by metabolism of infused U-^{13}C succinate (unlabeled: purple-rimmed unfilled circles). The abundance of ^{13}C-labeled metabolites downstream of succinate (m+4 fumarate (**G**), m+4 malate (**H**), m+4 citrate (**I**), m+4 aspartate (**J**), and m+3 pyruvate (**K**)) relative to m+4 succinate is respectively represented. Red horizontal lines with error bars report the mean ± SEM.

m+4 succinate levels were significantly lower than in liver, lung, BAT, WAT, and blood. We estimated succinate turnover in these tissues from the m+4 labeled fraction. As expected all tissues accumulated significantly less m+4 succinate fractional labeling. We compared succinate labeling in each tissue to the retina as a reference tissue that accumulates little succinate labeling. Fractional succinate labeling was significantly higher in eyecup, lung, BAT, and WAT than retina (**Figure 2D**).

Fractional labeling reports the turnover of the pool in a tissue so it depends on import relative to overall succinate pool size. A low fractional labeling does not necessarily mean a tissue is not metabolizing succinate. We therefore estimated succinate catabolism by summing the molar abundance of ^{13}C (originating from U-^{13}C-succinate) on all metabolites that we routinely measure (**Table 2**). We normalized this quantity to the molar abundance of ^{12}C in the same sample (**Figure 2E**). Compared to the retina, $^{13}C/^{12}C$ was significantly greater in eyecup, brown adipose tissue, and blood.

^{13}C from succinate labeled downstream intermediates in the conventional Krebs cycle, indicating active succinate oxidation. These include fumarate, malate, aspartate, citrate, and pyruvate. **Figure 2F** shows the isotopologues of these intermediates expected to appear in tissues following conventional Krebs cycle-mediated succinate catabolism. Enrichment of ^{13}C on these metabolites depends on the amount of m+4 succinate present in each tissue (**Figure S3**). To compare how different tissues use succinate, we normalized the abundance of these labeled metabolites to m+4 succinate. 5-minutes post-infusion, downstream mitochondrial metabolites are ^{13}C-labeled, with relatively low labeling in blood (**Figure 2G-K**). All tissues accumulated significantly higher ratio of m+4 fumarate/m+4 succinate than blood, and a significantly lower ratio of m+4 fumarate/m+4 succinate than eyecups. This implies that succinate oxidation may be faster in eyecup tissue than in others (**Figure 2G**). M+4 fumarate/m+4 succinate in retina was about the same as in other tissues (**Figure 2G**), suggesting that the poor response of retina OCR to succinate observed *ex vivo* reflects slower succinate import rather than oxidation. Higher m+4 fumarate in eyecups also leads to more ^{13}C in downstream intermediates such as malate (**Figure 2H**), citrate (**Figure 2I**), and aspartate (**Figure 2J**). These data could suggest that SDH is more abundant or more active in eyecups than other tissues. We performed immunoblots to determine the relative abundances of complex I, II, III, IV and V (ATP synthase) component proteins (NDUFS8, SDHB, UQCRC2, mt-CO1, and ATP5A). Levels of the Complex II component SDHB in eyecups are equal to or lower than in most other tested tissues. This suggests that m+4 fumarate labeling is not linked directly to expression of SDHB (**Figure S4**).

While retina succinate import is relatively slow, it does occur and can be detected by m+4 labeling of Krebs cycle intermediates. We reasoned that poor succinate import may be a sign that there are other differences in the way retina tissue handles m+4 succinate. We found that m+3 pyruvate/m+4 succinate was significantly higher in the retina than other tissues (**Figure 2K**), which may be indicative of substantial malic enzyme (*ME*) activity or phosphoenolpyruvate carboxykinase (PEPCK) activity in the retina. Both of these are able to form m+3 pyruvate, either from m+4 malate m+3 pyruvate (ME), or from m+4 oxaloacetate m+3 PEP m+3 pyruvate (*PEPCK* and pyruvate kinase).

Succinate Infusion Reveals Specialized Metabolic Features in the Retina and Eyecup

Succinate catabolism appeared to be unique in the retina, so we followed ^{13}C labeling in the retina and adjacent eyecup tissue 1, 2, 3, 5, and 12 minutes following infusion of 100 mg/kg U-^{13}C succinate. M+0 and m+4 succinate are the principal isotopologues following infusion. These species decay following the bolus infusion as ^{13}C-succinate carbons flow into different metabolic pathways. This decay suggests that in the 11 minutes following infusion, ~44% of the eyecup succinate pool is m+4 labeled then replaced by unlabeled succinate (**Figure 3A**) Only ~5% of the succinate pool is m+4 labeled then replaced in retinas (**Figure 3B**). As a consequence of higher

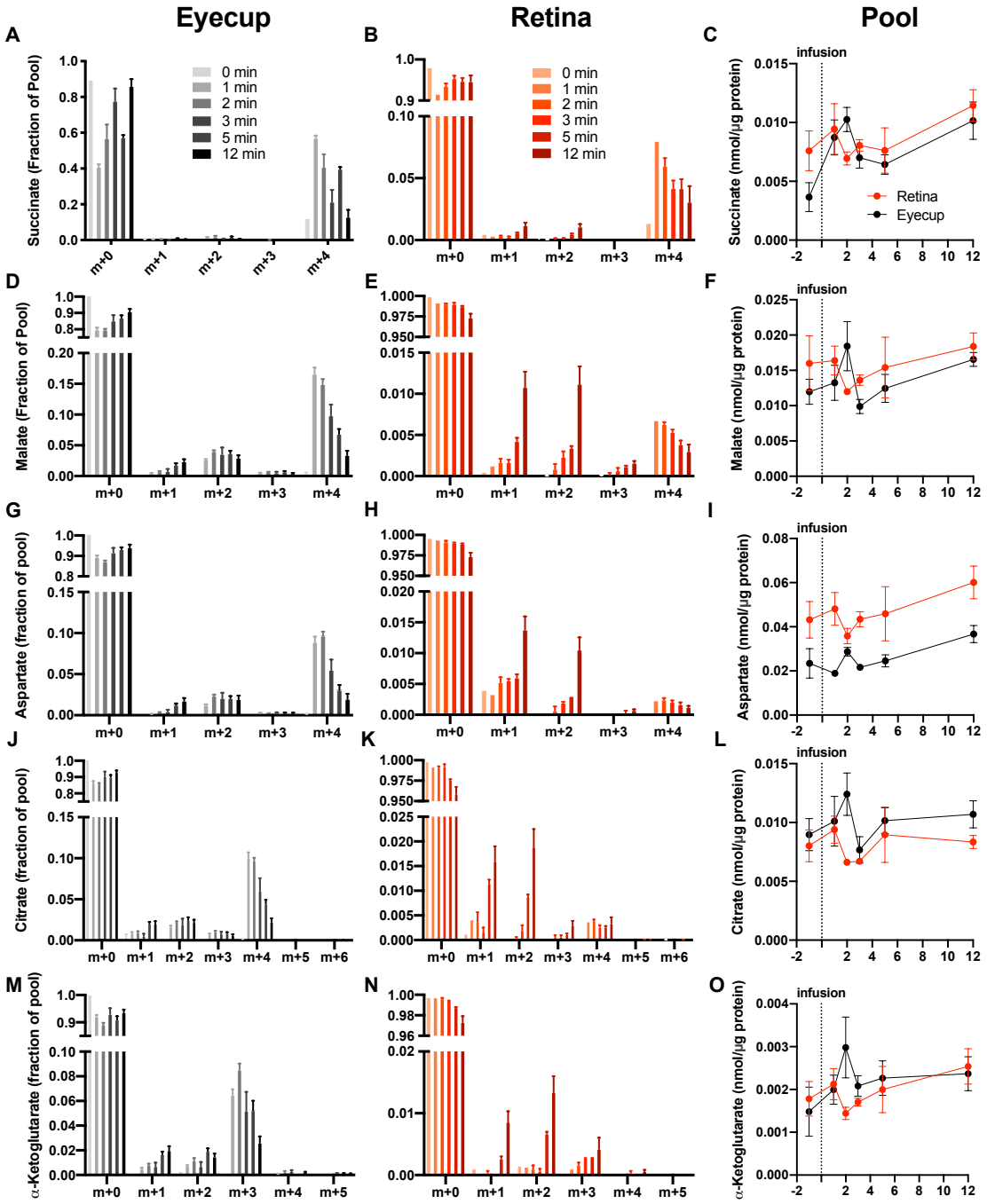

Figure 3. Infused Succinate Reveals Diverse Metabolic Routes in the Retina and Eyecup. Following bloodstream infusion of U-^{13}C-succinate in retina and eyecup, we determined the fractional labeling (**A-B, D-E, G-H, M-N**) and total abundance (metabolite pool size; **C, F, I, L, O**) of succinate (**A-C**), malate (**D-F**), aspartate (**G-I**), citrate (**J-L**), and α-ketoglutarate (**M-O**) 1, 2, 3, 5, and 12 minutes post-infusion. We compared these to labeling of tissue from un-infused catheterized C57BL6/J mice ("0 minutes"). M+*x* indicates that the molecule is ^{13}C-labeled with *x* carbons, all originating from infused succinate. N=3 for all time points except 12 minutes post-infusion, where n=6. All bars and dots represent mean ± SEM.

m+4 succinate turnover in eyecups, downstream m+4 or m+3 isotopologues of malate (**Figure 3D**), aspartate (**Figure 3G**), citrate (**Figure 3J**), α-ketoglutarate (**Figure 3M**), isocitrate (**Figure S5A**), and glutamate **(Figure S5D)** accumulate more rapidly in eyecup than in retina, showing that the conventional Krebs cycle is highly active in this tissue. Lesser ^{13}C-succinate import to the retina yields lower fractional ^{13}C labeling in downstream intermediates such as malate and citrate (**Figure 3E,K**).

Poor ^{13}C labeling in the Krebs cycle intermediates could indicate that ^{13}C from succinate was following a different route in the retina. The absence of m+4 aspartate or citrate suggested that oxaloacetate is diverted away from reactions that form citrate or aspartate. We investigated alternate metabolic pathways for malate carbons by following ^{13}C labeling on glycolytic intermediates and found that, similar to m+3 pyruvate/m+4 succinate, m+3 PEP/ m+4 succinate is high in retina and eyecup tissue compared to all the other tissues (**Figure 4A**). A closer investigation revealed that m+3 labeling accumulates on pyruvate, phosphoenolpyruvate (PEP), and 3-phosphoglycerate (3PG) over time in both retina and eyecup tissue (**Figure 4C-K**). Accumulation of ^{13}C from succinate on these intermediates suggests that these tissues are performing the initial steps of gluconeogenesis, including the *PEPCK* and pyruvate carboxylase (*PC*) reactions. *PEPCK* catalyzes decarboxylation of oxaloacetate (m+4 labeled if its carbons originated as infused succinate) to form m+3 phosphoenolpyruvate and m+1 CO_2. The PEP can become m+3 3PG through the reversible steps of glycolysis, or m+3 pyruvate through either pyruvate kinase or *ME*. In eyecups the succinate pool is more labeled but the 3PG pool is less labeled than in retinas. This indicates that there is more gluconeogenic activity in the retina than in the eyecup. We were concerned that m+3 labeling on glycolytic intermediates was derived from ^{13}C labeled glucose made by gluconeogenesis in the liver. However, the animals used in these experiments were not fasted and we found that the livers of infused mice had no detectable m+3 gluconeogenic intermediates (**Figure 4A**).

Decarboxylation of m+4 oxaloacetate by PEPCK, m+3 pyruvate by PDH, m+4 isocitrate by isocitrate dehydrogenase, or m+4 α-ketoglutarate by α-ketoglutarate dehydrogenase generates m+1 CO_2, and pyruvate carboxylation can transfer this m+1 CO_2 to generate an m+1 labeled metabolite. Therefore the time-dependent accumulation of m+1 α-ketoglutarate, isocitrate, citrate, and malate is consistent with *PC* activity, usually present in gluconeogenic tissues alongside *PEPCK* (**Figure 3**). The data that suggests gluconeogenic enzyme activity that can be probed *in vivo* using ^{13}C-succinate. We tested whether these activities also occur in isolated tissues. We incubated explanted retinas and eyecups in 5 mM glucose + 50 μM U-^{13}C succinate for 0, 0.5, 1, 2, and 5 minutes. The tissues were metabolically active and imported the labeled succinate, yet they did not form m+3 3-PG, suggesting that the factors enable gluconeogenesis *in vivo* are not recapitulated in our *ex vivo* culture system (**Figure S6**).

Succinate Stimulates Mitochondrial Uncoupling in Eyecup Tissue Isotopologues

Our analyses of ^{13}C succinate flux shows flux into gluconeogenic precursors in the retina and highly active oxidation in most tissues including the eyecup (**Figures 1G, 2D, 2E, and 3**). The extent to which increasing concentrations of succinate stimulate mitochondrial O_2 consumption (**Figure 1**) is surprising, as the capacity of tissues to oxidize mitochondrial substrates usually is constrained by the buildup of mitochondrial proton motive force (Δρ). Substrate oxidation increases Δρ, which opposes further substrate oxidation. We validated this with the conventional mitochondrial substrate pair pyruvate/malate. By increasing the concentration of these substrates and measuring eyecup OCR, we showed that these O_2 consumption fueled by NADH-linked substrates is limited and saturates at ~3 mM pyruvate + 3 mM malate (**Figure 5A**).

Succinate oxidation also increases OCR, but eyecup succinate oxidation reaches its V_{max} at a higher substrate concentration (~30 mM, **Figure 1**). However, succinate and NADH promote different levels of mitochondrial H^+ flux per O_2 molecule. We converted substrate-dependent OCR

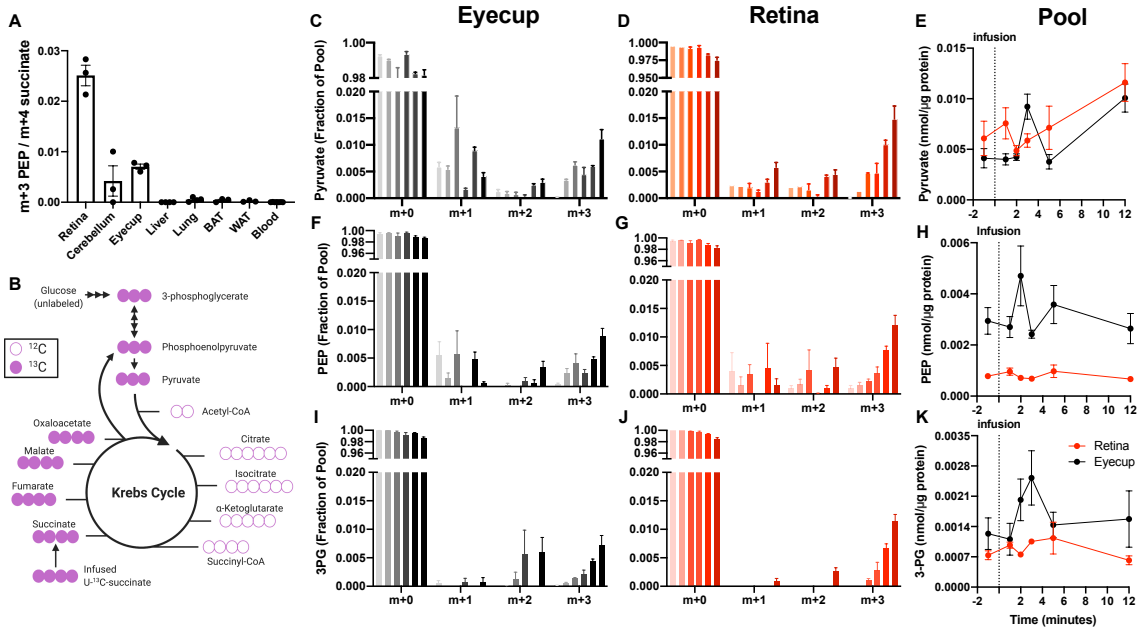

Figure 4. Infused Succinate Is Utilized to Make Glycolytic Precursors in Retina and Eyecup Tissue. (A) We determined m+3 phosphoenolpyruvate / m+4 succinate in our tissue panel 5 minutes following infusion, displaying data as in Figure 2G-K, **(B)** Schematic of the metabolic route by which ^{13}C-succinate is most likely able to label glycolytic intermediates**. (C-K)** We performed the same analysis as in Figure 3 on pyruvate (**C-E**), phosphoenolpyruvate (PEP; **F-H**), and 3-phosphoglycerate (3-PG; **I-K**). We compared these to labeling of tissue from un-infused catheterized C57BL6/J mice ("0 minutes"). M+*x* indicates that the molecule is ^{13}C-labeled with *x* carbons, all originating from infused succinate. N=3 for all time points except 12 minutes post-infusion, where n=6. All bars and dots represent mean ± SEM.

(**Figure 5A**) into estimates of H^+ flux, assuming (**1**) all OCR above the 5 mM glucose 'baseline' is from oxidation of the supplied substrate, and (**2**) each O_2 molecule consumed using NADH linked substrates catalyzed translocation of 10 $H^+/2e^-$ while succinate-dependent OCR translocated to an $H^+/2e^-$ ratio of 6 (**Figure 5B**). The effect of succinate and pyruvate/malate concentration on H^+ translocation overlapped at 300 μM and lower but deviated at ≥1 mM, with higher succinate concentrations inducing a greater H^+ flux than equimolar pyruvate/malate. The mismatch in OCR/H^+ flux suggests that exogenous succinate produces a H^+ leak across the inner mitochondrial membrane that is compensated for by additional substrate oxidation. We determined whether succinate produces H^+ leak by exposing eyecup tissue to either 5 mM succinate or 5 mM pyruvate/malate in the presence of the ATP synthase inhibitor oligomycin. O_2 consumption in the presence of oligomycin represents substrate oxidation that is not inhibited by Δρ. Leak respiration occurs at 5 mM of either substrate but is several fold greater when succinate rather than pyruvate/malate is used a fuel (**Figure 5C**).

We determined the extent to which succinate stimulates oligomycin-insensitive OCR by titrating succinate in the presence of oligomycin (**Figure 5D**). Succinate increases leak respiration at concentrations ≥ 300 μM. Multiple mechanisms could drive succinate dependent H^+ leak, including reactive oxygen species-induced activation of an uncoupling protein (Echtay et al., 2002; Mills et al., 2018), activation of H^+ leak through the adenine nucleotide translocase (ANT) (Bertholet et al., 2019), or activation of the mitochondrial permeability transition pore complex (mPTP) (Novgorodov et al., 1992). We stimulated succinate dependent H^+ leak by exposing eyecup tissue to 5 mM glucose, 10 μM oligomycin, and 5 mM succinate, and attempted to prevent succinate-stimulated leak respiration using inhibitors of oxidative stress (50 μM mitoTempo, 100 μM n-propyl gallate; **Figure 5E**), the ANT (30 μM carboxyatractyloside; **Figure 5F**), or the mPTP complex (2 μM cyclosporine A; **Figure 5G**). None of these compounds suppressed succinate-dependent leak respiration. We also tested whether succinate-dependent leak respiration occurs due to reverse complex I activity, which could oxidize coenzyme Q_{10}, reduce NAD^+, and transport H^+ from the mitochondrial intermembrane space to the matrix. The complex I Q-site inhibitor rotenone partially suppressed leak respiration (**Figure 5H**). We initially considered this to be a consequence of inhibiting complex I reversal fueled by succinate-dependent reduction of the coenzyme Q_{10} pool. However, the effect of rotenone also could be explained by cutting off the supply of electrons from glucose-derived NADH that can fuel OCR. We evaluated the contribution of glucose to OCR by removing it from the medium. Glucose removal partially suppressed OCR and prevented rotenone from affecting OCR (**Figure 5I**). That indicates that the effect of succinate on H^+ leak is not caused by reversal of proton pumping through complex I.

Discussion

The concentration of circulating succinate reaches up to 150 μM with obesity and 200 μM with type-2-diabetes (Serena et al., 2018), 150 μM during exercise in humans (Hochachka & Dressendorfer, 1976), and in excess of 300 μM when seals are forced to dive and become hypoxic (Hochachka et al., 1975). Until now it has been unclear how tissues handle that succinate, with some groups contesting the idea that extracellular succinate impacts mitochondrial activity.

Here we report evidence that many tissues can take up succinate from the circulation and oxidize it. This is partly evidenced by data showing that succinate fuels respiration when delivered extracellularly to intact tissues (**Figure 1**). We supported this claim more definitively by also showing that tissues take up and metabolize succinate *in vivo*. Our findings are consistent with a report that succinate stimulates consumption of O_2 by explants of dog heart and rabbit kidney (Furchgott & Shorr, 1948). However they differ from reports that succinate does not stimulate O_2 consumption by cultured cells (Ehinger et al., 2016; MacDonald et al., 1989; Mills et al., 2018).

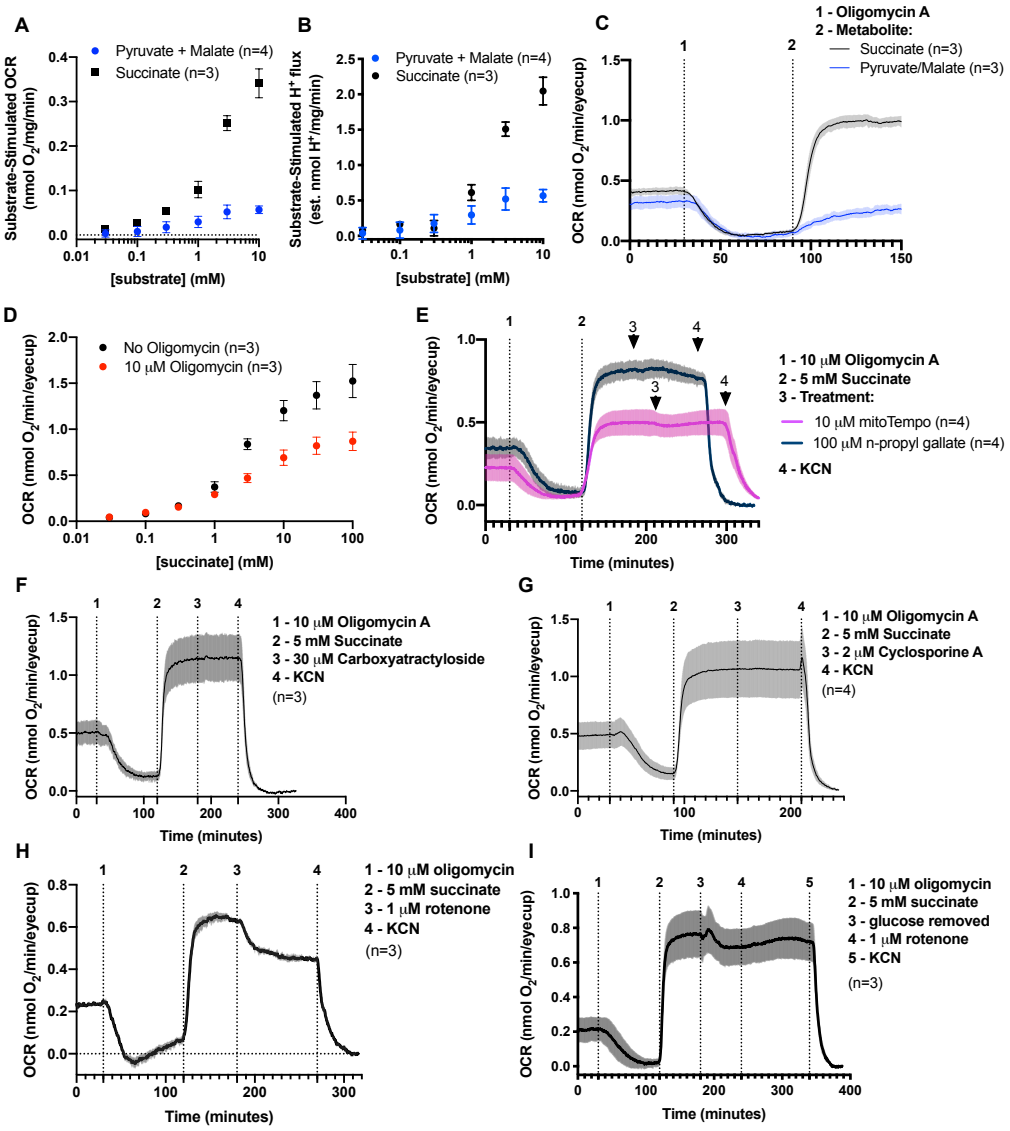

Figure 5. Extracellular Succinate Uncouples Eyecup Mitochondria *Ex Vivo*. (A) Eyecup OCR respiring on 5 mM glucose supplemented with increasing concentrations (30 μM, 100 μM, 300 μM, 1 mM, 3 mM, 10 mM) of succinate or malate and pyruvate. (**B**) We estimated mitochondrial H^+ flux from the matrix to the intermembrane space by multiplying OCR by the $H^+/2e^-$ ratio for the pyruvate/malate-linked substrate NADH (10) or succinate (6) (Hinkle et al., 1991). (**C**) We determined ATP synthase-independent substrate oxidation by incubating eyecup tissue in 5 mM glucose, then in 5 mM glucose with 10 μM of the ATP-synthase inhibitor oligomycin, and finally in a mix of 5 mM glucose, 10 μM oligomycin, and 5 mM of succinate (black) or pyruvate/malate (blue). (**D**) We determined how much respiration is oligomycin-resistant as a function of [succinate] (**E-I**) To determine the source of oligomycin-resistant respiration, we performed the treatments described in (C), but following the addition of 5 mM succinate we attempted to shut down the succinate-dependent increase in OCR by adding (**F**) the antioxidants mitotempo (purple line) or n-propyl gallate (black line), the adenine nucleotide translocator inhibitor carboxyatractyloside (CATR), (**G**) the mitochondrial permeability transition pore complex inhibitor cyclosporine A (CsA), (**H**) the mitochondrial complex I inhibitor rotenone, (**I**) or by removing glucose then adding rotenone. Lines represent mean O_2 consumption rate following subtraction of the 5 mM glucose "baseline" (**A,B,D**) or the 3 mM KCN "floor" (**C,E-I**).

Long-term cell culture can alter expression of metabolite transporters (Hanu et al., 2000). Diminished expression of succinate transporters could explain the differences between the metabolic responses of cultured cells compared to tissues.

We quantified succinate turnover (**Figure 2D**) and labeling of downstream metabolites with ^{13}C relative to ^{12}C (**Figure 2E**). These metrics show that succinate is oxidized to the greatest extent in eyecup, lung, and BAT. The ^{13}C-labeling metrics may underestimate succinate oxidation in eyecup, as the RPE may also import unlabeled succinate produced by the retina (Bisbach et al., 2020). Eyecup and lung tissue have high vascular access that may explain why m+4 succinate populates these pools so quickly. In BAT other mechanisms may contribute to rapid succinate utilization. For example, basal uncoupling could accelerate Krebs cycle activity so that succinate is oxidized quickly to fuel thermogenesis (Mills et al., 2018).

Both *in* and *ex vivo* the retina responds to succinate differently than other tissues. *Ex vivo*, succinate only slightly stimulates OCR (**Figure 1H**) and *in vivo* retina takes up less ^{13}C-succinate than other tissues (**Figure 2C-E**). Retina tissue explants export succinate (Bisbach et al., 2020), so the retina may favor succinate synthesis and export over import and oxidation. When imported to the retina, U-^{13}C-succinate m+3 labels PEP and 3PG. This distribution of ^{13}C likely results from a combination of the PEPCK reaction and reversible steps in glycolysis. We also noted that Krebs cycle intermediates become labeled with one ^{13}C (m+1, **Figure 3**). Pyruvate carboxylase (PC) can use $^{13}CO_2$ released by decarboxylation of Krebs cycle intermediates to make m+1 oxaloacetate. PEPCK and PC activities are both common beginning steps in gluconeogenesis. While this process occurs in retina and eyecup tissues, the proportion of ^{13}C incorporated into these intermediates relative to ^{13}C-succinate entry is more substantial in retinas than eyecups (**Figure 4**).

Succinate oxidation and downstream Krebs cycle activity are rapid in eyecups (**Figure 2**). That is surprising because succinate-dependent electron flux through complexes III and IV increase the proton-motive force (Δρ). Normally, a high Δρ limits respiration because electron transport couples directly coupled to H^+ pumping. Oligomycin blocks influx of protons through ATP synthase. Normally this causes Δρ to build to the point where electron transport stops (State 4, (Brand & Nicholls, 2011; Chance & Williams, 1955)). It is well-known that the effect of oligomycin is overcome by protonophore 'uncouplers' that dissipate the proton gradient.

Oligomycin stops glucose-stimulated respiration in eyecup tissue as expected. However, we were surprised to find that succinate overcomes this effect. This suggests that succinate may partially dissipate Δρ. The NADH-linked substrates pyruvate and malate do not have the same effect as succinate, suggesting that the apparent H^+ leak is unique to the biochemistry of succinate (**Figure 5A-B**). Others have noticed tis effect in BAT (Mills et al., 2018), but attribute uncoupling to free-radical dependent UCP1 activity. In our system succinate uncoupling is resistant to inhibitors of free radicals, ANT, and the mPTP, suggesting a unique mechanism of action that is effective even at low extracellular concentrations (<100 μM) (**Figure 5D-G**). That uncoupling can occur at relatively low concentrations is particularly important in the context of the eye. The retina releases succinate (Bisbach et al., 2020) and is proximal to eyecup tissue. Taken together our findings suggest that succinate released from the retina may accumulate to sufficient concentrations within the subretinal space to stimulate mitochondrial uncoupling in eyecups under physiological conditions.

Understanding the molecular mechanism that underlies succinate-dependent uncoupling will require further investigation. While we focus on eyecup tissue in this study, previous reports have demonstrated an exponential relationship between Δρ and H^+ leak in isolated mitochondria, particularly when the mitochondrial membrane is hyperpolarized (Brown & Brand, 1986; Nicholls, 1974). Increasing succinate flux increases the polarity of the mitochondrial membrane, and consequently, H^+ leak. Nicholls has proposed that Δρ-dependent dielectric breakdown of the

mitochondrial membrane causes this H^+ leak (Nicholls, 1974). This mechanism of action for succinate will be challenging to test conclusively in tissue. Follow-up investigations of our findings should develop new strategies to identify the molecular and biophysical mechanism of succinate-induced uncoupling.

Materials and Methods

Ethical Approval

This study was carried out in accordance with the National Research Council's Guide for the Care and Use of Laboratory Animals (*8th ed*). All protocols were approved by the Institutional Animal Care and Use Committees at the University of Washington and the VA Puget Sound Hospital.

Animals

All experiments used 2-5 month-old male and female wild-type C57BL6/J mice. These mice were housed at an ambient temperature of 25°C, with a 12-hour light cycle and *ad libitum* access to water and normal rodent chow.

Small animal surgeries

The procedure for chronic jugular vein and carotid artery catheterization was performed as previously described (Ayala et al., 2011) by the Cell Function and Analysis Core of the University of Washington's Diabetes Research Center. Briefly, following induction and maintenance under systemic inhaled anesthesia (isoflurane 1.5-2% in 1L/min), mice were administered with 4 mg/kg ketoprofen to reduce post-surgical swelling and provide analgesia. For intravenous infusions, jugular veins were isolated through a lateral incision to the trachea, and a silastic catheter was introduced into the vein, anchored to surrounding tissue, tunneled subcutaneously to the nape of the neck and connected to a vascular access port. A subset of mice received a contralateral carotid artery cannulation for blood sampling. The catheters were filled with heparinized saline, the skin incisions were sutured, and the mice recovered for 1 week before conscious infusion studies.

In vivo infusions

Jugular vein infusion studies were performed on freely moving, chronically cannulated mice. This system allowed us to avoid the potential confounding effects of acute surgical stress (Walters et al., 1992) or anesthesia (Windeløv et al., 2016) on succinate uptake or metabolism. We infused 100 mg/kg U-^{13}C-succinate (Cambridge Isotopes, CLM-1571) through jugular catheters over a period of approximately 20 seconds and euthanized awake mice by cervical dislocation 1, 2, 3, 5, or 10 minutes following the infusion. When mice possessed both carotid artery and jugular vein catheters, we took two 10 µL baseline blood samples per mouse then infused 100 mg/kg U-^{13}C-succinate through the jugular catheter. We sampled 10 µL of blood 0.5, 1, 2, 3, 4, 5, 7.5, and 10 minutes following the infusion, then euthanized mice. Following euthanasia we quickly dissected retinas and eyecups (a complex of the retinal pigment epithelium, sclera, and choroid vasculature) from the eye. For the 5 minutes post-infusion time point, we also dissected liver, lung, cerebellum, interscapular white adipose tissue, and interscapular brown adipose tissue. Dissected tissues were snap frozen in liquid N_2. All mice were euthanized between 10 AM and 1 PM to minimize circadian effects on metabolic function.

Ex vivo metabolic flux

In all *ex vivo* labeling experiments, we quickly euthanized mice by awake cervical dislocation, dissected the indicated tissues in Hank's Buffered Salt Solution (HBSS; GIBCO, Cat#: 14025-

076), and incubated them in pH 7.4 Krebs-Ringer bicarbonate (KRB) buffer (98.5 mM NaCl, 4.9 mM KCl, 1.2 mM KH_2PO_4 1.2 mM $MgSO_4$-$7H_2O$, 20 mM HEPES, 2.6 mM $CaCl_2$-$2H_2O$, 25.9 mM $NaHCO_3$) supplemented with 5 mM glucose and [U-^{13}C]-succinic acid (Cambridge isotope CLM-1571-0.1; concentrations indicated in figures). This buffer was pre-equilibrated at 37°C, 21% O_2, and 5% CO_2 prior to incubations. Following incubations, tissue was flash frozen in liquid N_2.

Metabolite Extraction

Metabolites were extracted using 80% MeOH, 20% H_2O supplemented with 10 µM methylsuccinate (Sigma, M81209) as an internal standard to adjust for any metabolite loss during the extraction and derivatization procedures. The extraction buffer was equilibrated on dry ice, and 150 µL was added to each sample. Tissues were then disrupted by sonication and incubated on dry ice for 45 minutes to precipitate protein. Proteins were pelleted at 17,000 x g for 30 minutes at 4°C. The supernatant containing metabolites was lyophilized at room-temperature until dry and stored at -80°C until derivatization. The pellet containing protein was resuspended by sonication in RIPA buffer (150 mM NaCl, 1.0% Triton X-100, 0.5% sodium deoxycholate, 0.1% SDS, 50 mM Tris, pH 8.0) and the amount of protein was determined by a BCA assay (ThermoFisher, 23225).

Metabolite Derivatization

Lyophilized samples were first derivatized in 10 µL of 20 mg/mL methoxyamine HCl (Sigma, Cat#: 226904) dissolved in pyridine (Sigma, Cat#: 270970) at 37°C for 90 minutes, and subsequently with 10 µL tert-butyldimethylsilyl-N-methyltrifluoroacetamide (Sigma, Cat#: 394882) at 70°C for 60 minutes.

Gas Chromatography-Mass Spectrometry

Metabolites were analyzed on an Agilent 7890/5975C GC-MS using selected-ion monitoring methods described extensively in previous work (Du et al., 2015). Peaks were integrated in MSD ChemStation (Agilent), and correction for natural isotope abundance was performed using the software IsoCor (Millard et al., 2019). Corrected metabolite signals were converted to molar amounts by comparing metabolite peak abundances in samples with those in a 'standard mix' containing known quantities of metabolites we routinely measure. Multiple concentrations of this mix were extracted, derivatized, and run alongside samples in each experiment. These known metabolite concentrations were used to generate a standard curve which allowed for metabolite quantification. Metabolite abundance was normalized to tissue protein concentration, and following this, paired tissues such as retinas and eyecups from the same mouse were treated as technical replicates and averaged.

Ex vivo oxygen consumption

Following euthanasia, mouse tissues were dissected and cut into small segments in Hank's buffered salt solution. These tissues were incubated in Krebs-Ringer bicarbonate buffer (KRB) supplemented with 5 mM glucose and pre-equilibrated at 37°C and 5% CO_2. We determined OCR using a custom-built perifusion flow-culture system (Neal et al., 2015; Sweet et al., 2002). Tissues were perifused in chambers between Cytopore beads (Amersham Biosciences, Piscatawy, NJ) and porous frits. With KRB supplemented with 5 mM glucose, 1x Antibiotic-Antimycotic (Gibco), and 1 mg/mL fatty acid-free bovine serum albumin. An artificial lung oxygenated supplemented KRB with a mixture of 21% O_2, 5% CO_2, and 74% N_2.Oxygenated media was passed through a bubble trap before exposure to mouse tissues. Outflow media came into contact with a glass wall coated with a thin layer of oxygen sensitive polymerized Pt(II) Meso-tetra(pentafluorophenyl)porphine dye (Frontier Scientific, Logan, UT) painted on the inner glass wall of the chamber. Following a 405 nm light pulse, the dye-coated glass emits a phosphorescent signal detected at 650 nm. The decay lifetime is dependent on oxygen tension.

The flow rate of KRB along with the quantitative relationship between dye phosphorescent decay and oxygen concentration were used to determine tissue OCR. All OCR measurements were obtained under control conditions (baseline, 5 mM glucose), one or more experimental conditions, and a 'zeroed' condition wherein 3 mM potassium cyanide (KCN) was used to directly inhibit complex IV and thus subtract the effect of residual non-mitochondrial oxygen consumption from our measurements.

Western Blot

Protein was extracted by sonication in RIPA buffer supplemented with a protease and phosphatase inhibitor cocktails (ThermoFisher, Cat#: 78442). SDS sample buffer was added and samples were run on 13% polyacrylamide gels. After running, gels were transferred onto PVDF membranes (Millipore, IPFL00010) and rinsed with PBS. Primary antibody (anti-Total Oxphos, 1:1000 dilution, RRID: AB_2629281, Lot# P3338) was diluted in blocking buffer (LI-COR, 927–40,000) and incubated overnight on blots at 4°C. Membranes were washed twice with PBS containing 0.1% Tween-20 and once with PBS, then incubated with secondary antibody (IRDye 800CW goat anti-mouse IgG (H + L) (LI- COR Biosciences, 925-32210, RRID: AB_2687825) at 1:5000 in blocking buffer for 1 h at RT and washed again before imaging. Membranes were imaged and bands were quantified using the LI-COR Odyssey CLx Imaging System (RRID:SCR_014579).

Statistical Analysis

We performed all statistical data analyses using Prism Version 8 (GraphPad Software). The significance threshold was set at $p<0.05$. In all figures, *$p<0.05$, **$p<0.01$, ***$p<0.001$, and ****$p<0.0001$. *(Figure 1)* To fit curves of oxygen consumption as a function of [succinate], for each sample we averaged steady-state oxygen consumption over >5 minutes at the end of a given treatment. These averaged values were considered to be the OCR at each given [succinate] for each sample. We fit the curve to an allosteric sigmoidal shape in order to obtain approximations of V_{max}, $K_{1/2}$, and Hill's coefficient (h) (Table 1). *(Figure 2)* We estimated the half-life of infused m+4 succinate in blood by a one-phase decay function to the data. The abundance (*Figure* 2C), fractional labeling (*Figure* 2D), and ratios of metabolite isotopologues (*Figure 2E*) were compared using a one-way ANOVA. *(Figure 5)* We analyzed differences in respiration following treatments using one-way ANOVAs . The values input into these ANOVAs are averaged steady-state oxygen consumption over >5 minutes at the end of a given treatment.

Acknowledgments

The authors thank Susan Brockerhoff, Ph.D. and Michelle Giarmarco, Ph.D. for their help in editing this manuscript. This research was supported by funding from the following sources T32 EY007031/EY/NEI NIH HHS/United States (to DTH), F31 EY031165/EY/NEI NIH HHS/United States (to CMB), R01 EY006641/EY/NEI NIH HHS/United States (to JBH), R01 EY017863/EY/NEI NIH HHS/United States (to JBH). OCR studies and conscious jugular infusion studies were performed at the Cell Function Analysis Core of the Univ. of Washington's Diabetes Research Center, which is supported by P30 DK017047/DK/NIDDK NIH HHS/United States.

Competing Interest Statement

The authors declare no competing interests.

References

Ayala, J. E., Bracy, D. P., Malabanan, C., James, F. D., Ansari, T., Fueger, P. T., McGuinness, O. P., & Wasserman, D. H. (2011, Nov). Hyperinsulinemic-euglycemic clamps in conscious, unrestrained mice. *J Vis Exp*(57). https://doi.org/10.3791/3188

Bertholet, A. M., Chouchani, E. T., Kazak, L., Angelin, A., Fedorenko, A., Long, J. Z., Vidoni, S., Garrity, R., Cho, J., Terada, N., Wallace, D. C., Spiegelman, B. M., & Kirichok, Y. (2019, 07). H+ transport is an integral functi°n of the mitochondrial ADP/ATP carrier. *Nature, 571*(7766), 515-520. https://doi.org/10.1038/s41586-019-1400-3

Bisbach, C. M., Hass, D. T., Robbings, B. M., Rountree, A. M., Sadilek, M., Sweet, I. R., & Hurley, J. B. (2020, May). Succinate Can Shuttle Reducing Power from the Hypoxic Retina to the O2 Rich Pigment Epithelium. *Cell Rep, 31*(5), 107606. https://doi.org/10.1016/j.celrep.2020.107606

Brand, M. D., & Nicholls, D. G. (2011, Apr). Assessing mitochondrial dysfunction in cells. *Biochem J, 435*(2), 297-312. https://doi.org/10.1042/BJ20110162

Brown, G. C., & Brand, M. D. (1986, Feb). Changes in permeability to protons and other cations at high proton motive force in rat liver mitochondria. *Biochem J, 234*(1), 75-81. https://doi.org/10.1042/bj2340075

Chance, B., & Williams, G. R. (1955, Nov). Respiratory enzymes in oxidative phosphorylation. I. Kinetics of oxygen utilization. *J Biol Chem, 217*(1), 383-393. https://www.ncbi.nlm.nih.gov/pubmed/13271402

Chouchani, E. T., Pell, V. R., Gaude, E., Aksentijević, D., Sundier, S. Y., Robb, E. L., Logan, A., Nadtochiy, S. M., Ord, E. N. J., Smith, A. C., Eyassu, F., Shirley, R., Hu, C. H., Dare, A. J., James, A. M., Rogatti, S., Hartley, R. C., Eaton, S., Costa, A. S. H., Brookes, P. S., Davidson, S. M., Duchen, M. R., Saeb-Parsy, K., Shattock, M. J., Robinson, A. J., Work, L. M., Frezza, C., Krieg, T., & Murphy, M. P. (2014, Nov). Ischaemic accumulation of succinate controls reperfusion injury through mitochondrial ROS. *Nature, 515*(7527), 431-435. https://doi.org/10.1038/nature13909

Du, J., Linton, J. D., & Hurley, J. B. (2015). Probing Metabolism in the Intact Retina Using Stable Isotope Tracers. *Methods Enzymol, 561*, 149-170. https://doi.org/10.1016/bs.mie.2015.04.002

Echtay, K. S., Roussel, D., St-Pierre, J., Jekabsons, M. B., Cadenas, S., Stuart, J. A., Harper, J. A., Roebuck, S. J., Morrison, A., Pickering, S., Clapham, J. C., & Brand, M. D. (2002, Jan). Superoxide activates mitochondrial uncoupling proteins. *Nature, 415*(6867), 96-99. https://doi.org/10.1038/415096a

Ehinger, J. K., Piel, S., Ford, R., Karlsson, M., Sjövall, F., Frostner, E., Morota, S., Taylor, R. W., Turnbull, D. M., Cornell, C., Moss, S. J., Metzsch, C., Hansson, M. J., Fliri, H., & Elmér, E. (2016, 08). Cell-permeable succinate prodrugs bypass mitochondrial complex I deficiency. *Nat Commun, 7*, 12317. https://doi.org/10.1038/ncomms12317

Furchgott, R. F., & Shorr, E. (1948, Aug). The effect of succinate on respiration and certain metabolic processes of mammalian tissues at low oxygen tensions in vitro. *J Biol Chem, 175*(1), 201-215. https://www.ncbi.nlm.nih.gov/pubmed/18873295

Geubelle, P., Gilissen, J., Dilly, S., Poma, L., Dupuis, N., Laschet, C., Abboud, D., Inoue, A., Jouret, F., Pirotte, B., & Hanson, J. (2017, 05). Identification and pharmacological characterization of succinate receptor agonists. *Br J Pharmacol, 174*(9), 796-808. https://doi.org/10.1111/bph.13738

Hanu, R., McKenna, M., O'Neill, A., Resneck, W. G., & Bloch, R. J. (2000, May). Monocarboxylic acid transporters, MCT1 and MCT2, in cortical astrocytes in vitro and in vivo. *Am J Physiol Cell Physiol, 278*(5), C921-930. https://doi.org/10.1152/ajpcell.2000.278.5.C921

Hochachka, P. W., & Dressendorfer, R. H. (1976, Sep). Succinate accumulation in man during exercise. *Eur J Appl Physiol Occup Physiol, 35*(4), 235-242. https://doi.org/10.1007/BF00423282

Hochachka, P. W., Owen, T. G., Allen, J. F., & Whittow, G. C. (1975, Jan). Multiple end products of anaerobiosis in diving vertebrates. *Comp Biochem Physiol B, 50*(1), 17-22. https://doi.org/10.1016/0305-0491(75)90292-8

MacDonald, M. J., Fahien, L. A., Mertz, R. J., & Rana, R. S. (1989, Mar). Effect of esters of succinic acid and other citric acid cycle intermediates on insulin release and inositol phosphate formation by pancreatic islets. *Arch Biochem Biophys, 269*(2), 400-406. https://doi.org/10.1016/0003-9861(89)90123-9

Millard, P., Delépine, B., Guionnet, M., Heuillet, M., Bellvert, F., & Létisse, F. (2019, 11). IsoCor: isotope correction for high-resolution MS labeling experiments. *Bioinformatics, 35*(21), 4484-4487. https://doi.org/10.1093/bioinformatics/btz209

Mills, E. L., Pierce, K. A., Jedrychowski, M. P., Garrity, R., Winther, S., Vidoni, S., Yoneshiro, T., Spinelli, J. B., Lu, G. Z., Kazak, L., Banks, A. S., Haigis, M. C., Kajimura, S., Murphy, M. P., Gygi, S. P., Clish, C. B., & Chouchani, E. T. (2018, Aug). Accumulation of succinate controls activation of adipose tissue thermogenesis. *Nature, 560*(7716), 102-106. https://doi.org/10.1038/s41586-018-0353-2

Neal, A., Rountree, A. M., Philips, C. W., Kavanagh, T. J., Williams, D. P., Newham, P., Khalil, G., Cook, D. L., & Sweet, I. R. (2015, Dec). Quantification of Low-Level Drug Effects Using Real-Time, in vitro Measurement of Oxygen Consumption Rate. *Toxicol Sci, 148*(2), 594-602. https://doi.org/10.1093/toxsci/kfv208

Nicholls, D. G. (1974, Dec). The influence of respiration and ATP hydrolysis on the proton-electrochemical gradient across the inner membrane of rat-liver mitochondria as determined by ion distribution. *Eur J Biochem, 50*(1), 305-315. https://doi.org/10.1111/j.1432-1033.1974.tb03899.x

Novgorodov, S. A., Gudz, T. I., Milgrom, Y. M., & Brierley, G. P. (1992, Aug). The permeability transition in heart mitochondria is regulated synergistically by ADP and cyclosporin A. *J Biol Chem, 267*(23), 16274-16282. https://www.ncbi.nlm.nih.gov/pubmed/1644813

Prag, H. A., Gruszczyk, A. V., Huang, M. M., Beach, T. E., Young, T., Tronci, L., Nikitopoulou, E., Mulvey, J. F., Ascione, R., Hadjihambi, A., Shattock, M. J., Pellerin, L., Saeb-Parsy, K., Frezza, C., James, A. M., Krieg, T., Murphy, M. P., & Aksentijevic, D. (2020, Aug 7). Mechanism of succinate efflux upon reperfusion of the ischemic heart. *Cardiovasc Res*. https://doi.org/10.1093/cvr/cvaa148

Serena, C., Ceperuelo-Mallafré, V., Keiran, N., Queipo-Ortuño, M. I., Bernal, R., Gomez-Huelgas, R., Urpi-Sarda, M., Sabater, M., Pérez-Brocal, V., Andrés-Lacueva, C., Moya, A., Tinahones, F. J., Fernández-Real, J. M., Vendrell, J., & Fernández-Veledo, S. (2018, 06). Elevated circulating levels of succinate in human obesity are linked to specific gut microbiota. *ISME J, 12*(7), 1642-1657. https://doi.org/10.1038/s41396-018-0068-2

Sweet, I. R., Cook, D. L., Wiseman, R. W., Greenbaum, C. J., Lernmark, A., Matsumoto, S., Teague, J. C., & Krohn, K. A. (2002). Dynamic perifusion to maintain and assess isolated pancreatic islets. *Diabetes Technol Ther, 4*(1), 67-76. https://doi.org/10.1089/15209150252924111

Walters, J. M., Ward, G. M., Kalfas, A., Best, J. D., & Alford, F. P. (1992, Jun). The effect of epinephrine on glucose-mediated and insulin-mediated glucose disposal in insulin-dependent diabetes. *Metabolism, 41*(6), 671-677. https://doi.org/10.1016/0026-0495(92)90062-f

Wang, T., Xu, Y. Q., Yuan, Y. X., Xu, P. W., Zhang, C., Li, F., Wang, L. N., Yin, C., Zhang, L., Cai, X. C., Zhu, C. J., Xu, J. R., Liang, B. Q., Schaul, S., Xie, P. P., Yue, D., Liao, Z. R., Yu, L. L., Luo, L., Zhou, G., Yang, J. P., He, Z. H., Du, M., Zhou, Y. P., Deng, B. C., Wang, S. B., Gao, P., Zhu, X. T., Xi, Q. Y., Zhang, Y. L., Shu, G., & Jiang, Q. Y. (2020, May). Succinate induces skeletal muscle fiber remodeling via SUCNR1 signaling. *EMBO Rep, 21*(5), e50461. https://doi.org/10.15252/embr.202050461

Windeløv, J. A., Pedersen, J., & Holst, J. J. (2016, Jun). Use of anesthesia dramatically alters the oral glucose tolerance and insulin secretion in C57Bl/6 mice. *Physiol Rep, 4*(11). https://doi.org/10.14814/phy2.12824

1 **Table 2. Metabolites used to determine total ^{13}C labeling**

Metabolic process	Metabolite Name	# carbons
Glycolysis	Dihydroxyacetone phosphate	3
Glycolysis	3-phosphoglycerate	3
Glycolysis	Phosphoenolpyruvate	3
Glycolysis	Pyruvate	3
Krebs Cycle	Citrate	6
Krebs Cycle	Isocitrate	6
Krebs Cycle	α-ketoglutarate	5
Krebs Cycle	fumarate	4
Krebs Cycle	malate	4
Krebs Cycle (anapleurotic)	aspartate	4
Krebs Cycle (anapleurotic)	glutamate	5

2 *Although we routinely measure succinate, it was not included on this table because ^{13}C labeling
3 on succinate could be indicative of residual infusate in the cytosol or blood-vessels.

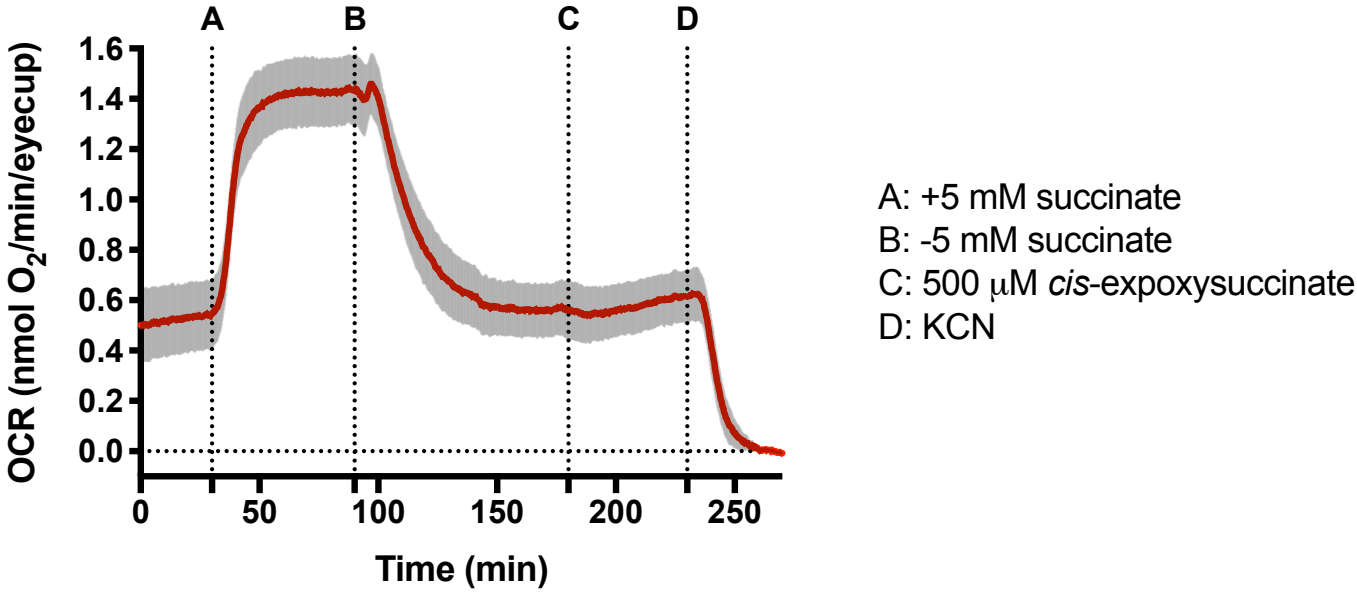

Figure S1. SUCNR1 Agonism is insufficient to increase oxygen consumption. Eyecup tissue was dissected from C57BL6J mice and ex vivo oxygen consumption rate (OCR, mean±SEM) measured as described in the materials and methods section. At baseline (0-30 minutes) the only source of energy to eyecups to fuel OCR was 5 mM glucose. At time=30 (A) minutes 5 mM succinate was added, which increased OCR ~3-fold. Succinate was withdrawn (B) and OCR fell to control values. *Cis*-epoxysuccinate is a SUCNR1 agonist with 10x greater potency for the GPCR than succinate (Geubelle et al., 2017). (C) We added 500 μM cis-epoxysuccinate to the 5 mM glucose treatment to determine whether any increases in OCR were due to metabolic changes transduced by SUCNR1. (D) KCN was used to inhibit mitochondrial complex IV OCR activity to confirm that the OCR observed in this experiment was primarally mitochondrial. We did not find any immediate effects of SUCNR1 agonism on OCR that were comparable to those of succinate itself, suggesting that succinate-induced OCR occurs mainly through direct succinate oxidation and not downstream protein signaling. (n=4)

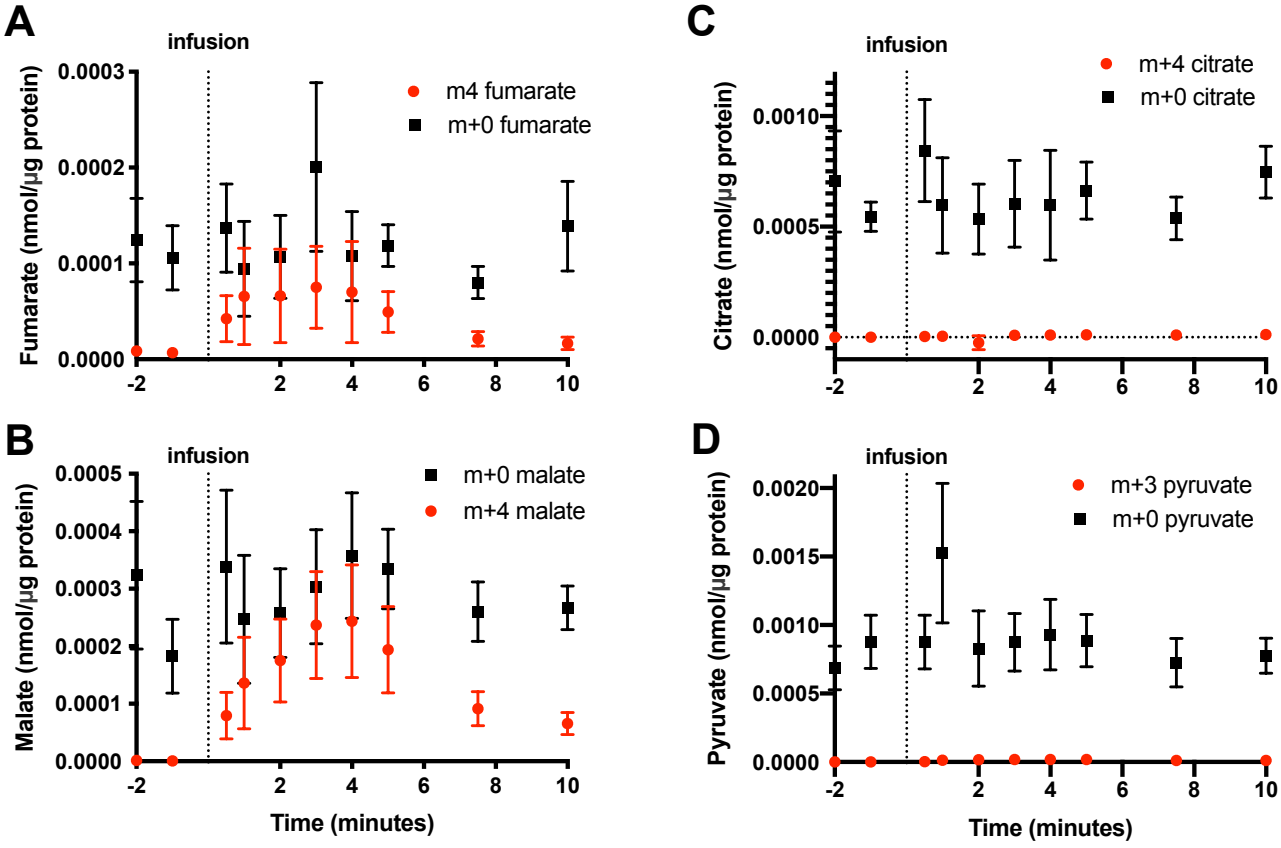

Figure S2. Post-Infusion blood Metabolite Labeling. U-^{13}C-succinate was infused into blood through a veinous catheter and 10 µL blood samples were drawn at 0.5, 1, 2, 3, 4, 5, 7.5, and 10 minutes post-infusion. Analysis of blood samples shows that following the infusion, succinate does turn over in whole blood to become (A) m+4 fumarate and (B) m+4 malate, while downstream (C) m+4 citrate and upstream (D) m+3 pyruvate appear relatively unperturbed, though this occurs to a far lesser extent than m+4 succinate turnover in blood, suggesting that rather than blood succinate feeding blood fumarate or malate pools, it is taken up into tissues. The formation of m+4 intermediates in blood does not appear to perturb the m+0 pools of unlabeled metabolic intermediates also in blood. (n=5-7)

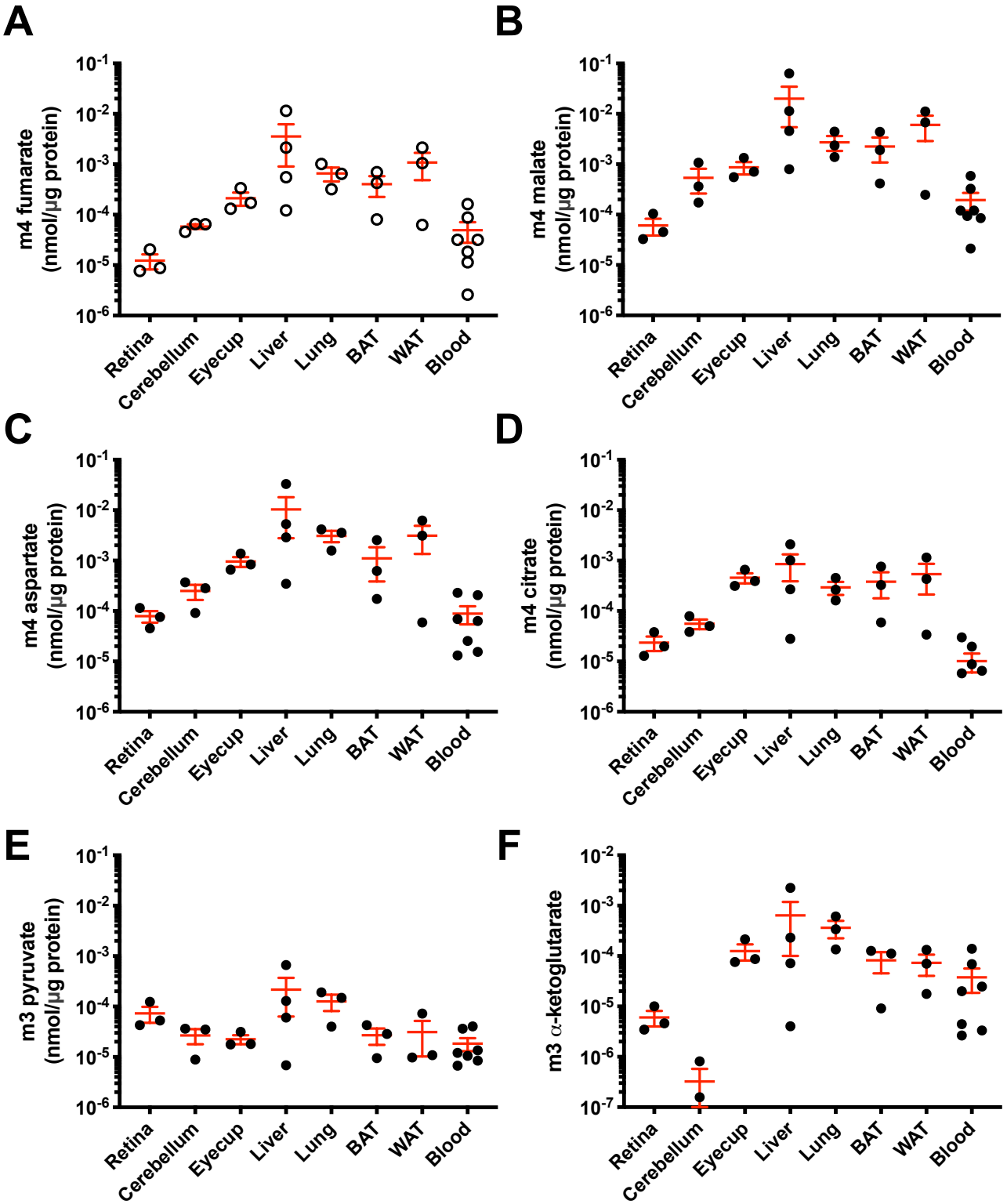

Figure S3. Abundance of labeled TCA cycle intermediates in various tissues 5 minutes following bloodstream succinate infusion. (A) m+4 fumarate, (B) m+4 malate, (C) m+4 aspartate, (D) m+4 citrate, (E) m+3 pyruvate, (F) and m+3 α–Ketoglutarate in retina, cerebellum, eyecup, liver, lung, BAT, WAT, and blood tissue. The labeling patterns of most downstream metabolic intermediates are subject to the amount of m+4 succinate imported into that tissue and thus the relative abundances of m+4 labeled matabolites closely matches that of m+4 succinate in tissues (n=3-4).

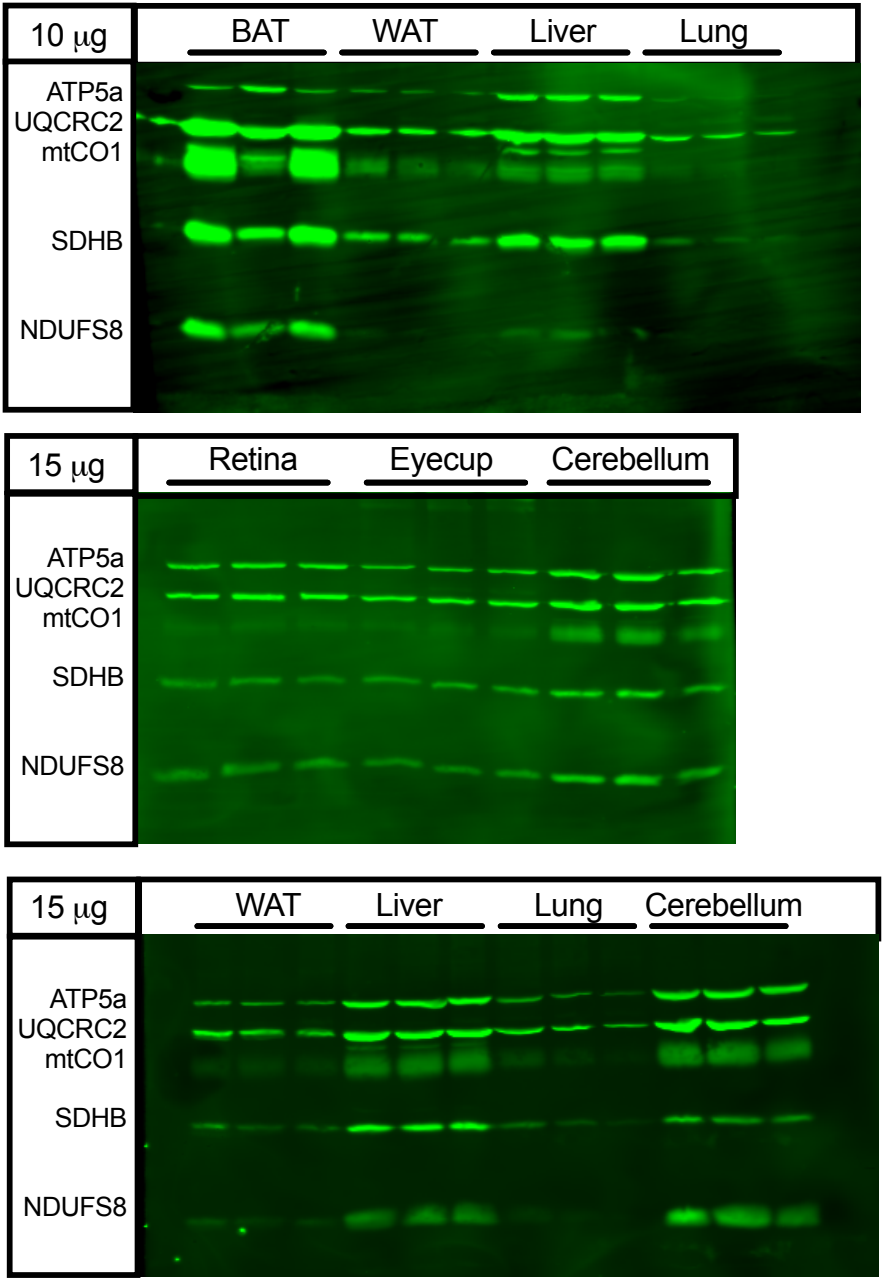

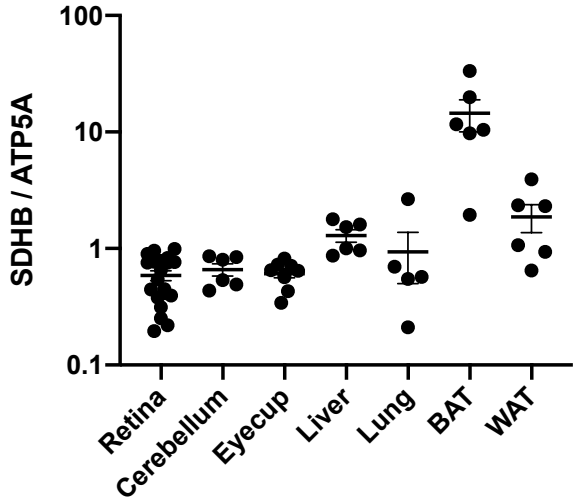

Figure S4. Mouse Succinate Dehydrogenase subunit B (SDHB) expression in a Panel of Tissues. Indicated tissues were dissected from young (~8 week old) C57BL6/J mice and lysed in RIPA buffer by sonication. Indicated protein amounts (top left corner of each blot) were loaded into and run on a 13% polyacrylamide gel, and transferred to a PVDF membrane prior to blocking and immunolabeling using a mouse anti-Total OXPHOS antibody (abcam, ab110413, diluted 1:1000). To determine mitochondrial SDHB levels, we normalized SDHB levels to those of the ATP synthase subunit ATP5a and plotted noramlized SDHB/ATP5a values for retina, cerebellum, eyecup, liver, lung, BAT, and WAT obtained across multiple blots. Mean±SEM, n=5-20, 1 outlying lung sample was excluded from this data.

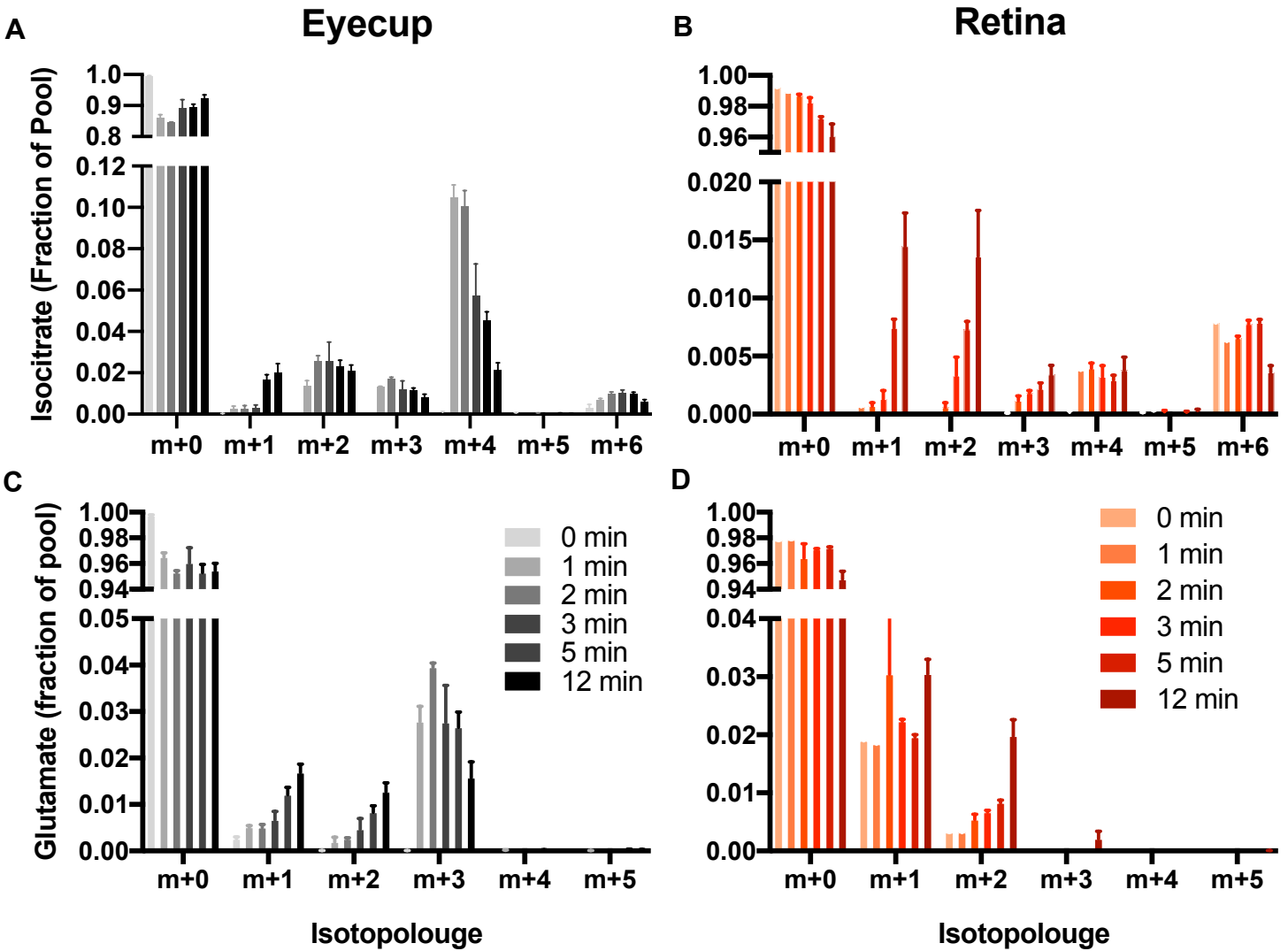

Figure S5. Isocitrate and Glutamate Isotopolouge Distributions in Retina and Eyecup Tissue Following *In Vivo* U-^{13}C-Succinate Infusion.

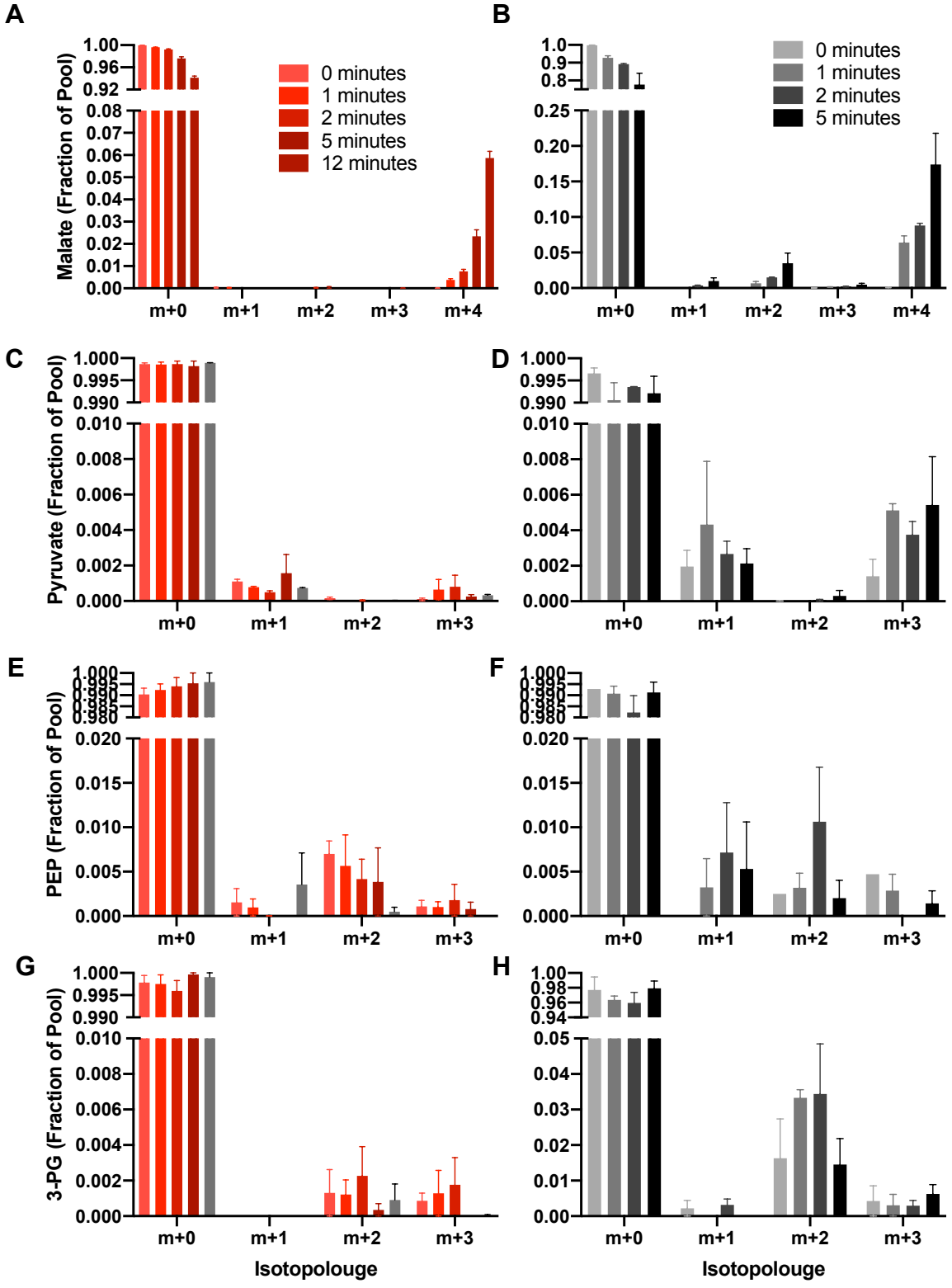

Figure S6. Lack of Gluconeogenesis in *Ex Vivo* Retina and Eyecup Tissue. Retina and Eyecup tissue was dissected from C57BL6/J mice in Hanks buffered salt solution. The tissue was next incubated in a Krebs-Ringer Bicarbonate Buffer supplemented with 5 mM glucose and 50 μM U-^{13}C-succinate equillibrated to 37°C at 5% CO_2 (n=1-3). Tissues were incubated in this buffer for 0, 1, 2, or 5 minutes and flash-frozen in liquid N_2. Tissue was homogenized, derivitized, and metabolite abundance determined using gas chromatography-mass spectrometry. Relative isotopolouge abundance was determined and is plotted for (A-B) malate, (C-D) pyruvate, (E-F) PEP, and (G-H) 3-PG. While carbons from labeled succinate do appear on Krebs cycle intermediates in both tissues (A-B) , they do not appear to accumulate m+3 labeling on Pyruvate, PEP, or 3-PG (C-H) linerarly over time as they do in vivo (Figure 4).